DFT+U study of electrical levels and migration barriers of early 3d and 4d transition metals in silicon

A. G. Marinopoulos,* P. Santos, and J. Coutinho
Department of Physics & I3N, University of Aveiro, 3810-193 Aveiro, Portugal
(Received 11 May 2015; revised manuscript received 17 June 2015; published 17 August 2015)

Owing to their strong interaction with carriers, early 3d-row (Ti, V, and Cr) and 4d-row (Zr, Nb, and Mo) transition metals (TMs) are undesired contaminants in solar- and electronic-grade Si. The increasing stringent control of contamination levels is urging an accurate picture of their electronic structure. In the present work, the electrical levels and migration energies of these TMs are determined by means of standard density-functional theory (DFT) and a rotationally invariant formulation of DFT+U. The latter approach improves on the treatment of electronic correlations at the TM sites and relies on on-site Hubbard Coulomb and Hund's exchange parameters U and J, respectively. These are calculated self-consistently from linear-response theory without fitting to experimental data. The effect of correlation was found more pronounced for Ti and V, with a strong impact on the location of their electrical levels. In most cases, the agreement with the experimental data is satisfactory allowing the identification of the type and character of the levels. For Cr and Mo in particular, the results resolve longstanding controversies concerning the type and position of the levels. The obtained migration barriers display moderate charge-state and correlation dependency. High barriers were found for all metals studied, with the exception of Cr, confirming them as slow diffusers in silicon among the whole TM family.

DOI: 10.1103/PhysRevB.92.075124 PACS number(s): 71.15.Mb, 71.20.Mq, 71.55.−i, 66.30.J−

I. INTRODUCTION

Understanding transition-metal (TM) impurities in semiconductors is simultaneously a problem with huge technological impact and a challenge in fundamental solid state physics. From a first-principles modeling perspective, the treatment of on-site correlations due to the d electrons on the TMs, implies a departure from standard local or semilocal approximations to account for electron-electron interactions [1]. Within density-functional theory (DFT), recently developed hybrid functionals, which admix a portion of exact nonlocal Fock exchange to the total exchange, have emerged as very accurate alternative approaches [2–4]. Nonetheless, they remain computationally expensive and they require by construction the tuning of a mixing parameter which defines the portion of the nonlocal exchange. Usually, this parameter is chosen in order to reproduce the experimental gap or other properties of the specific bulk system under study. However, the use of a unique parameter does not warrant a proper description of d-electron defect states induced by a TM impurity when the latter is inserted in a sp-bonded semiconducting host [5]. Indeed, recent studies of TM defects in semiconductors have shown that hybrid functionals led to insufficient screening of Coulomb interactions within the localized d electrons of the TMs, failing to reduce the self-interaction error [6,7]. The solution suggested by these authors was to apply an additional occupation-dependent potential to the d orbitals in order to satisfy a generalized Koopman's theorem.

In the present work, we explore the use of an affordable first-principles methodology for the treatment of on-site exchange and correlation effects in TM point defects in semiconductors. Our case study was chosen to be the early transition metals of the 3d and 4d rows in crystalline silicon. Such defects are feared contaminants in solar- and electronic-silicon technology [8], being powerful recombination centers when dispersed in the lattice as single interstitial defects [9]. Owing to their low diffusivity, limited precipitation and segregation under thermal treatments, they are perceived as particularly detrimental in silicon photovoltaics [8]. Early studies based on electron paramagnetic resonance (EPR) pioneered by Ludwig and Woodbury [10,11] were instrumental in resolving the hyperfine structure of the 3d-row metals in silicon and in identifying their electron spin state. Subsequent work by deep-level transient spectroscopy (DLTS) showed that both 3d- and 4d-row metals are electrically active and introduce several deep levels in the gap [8,9,12,13]. Hence, it is of primary interest to be able to determine accurately the properties of these TMs in silicon, in particular, the location of their electrical levels in the gap. Understanding migration mechanisms and determining their corresponding energy barriers can also lead to a better perception and control of the kinetic processes involving these metals, in particular during annealing and gettering treatments.

TM impurities in silicon were studied in the past using a variety of first-principles approaches. These included early calculations where the crystalline host was represented by finite-sized atomic clusters [14,15] and spin-unrestricted Green's function techniques [16–19] based on the atomic-sphere approximation. In spite of their contribution to the elucidation of the main trends regarding the electronic structure of the TMs (such as their ground-state spin configurations and the orbital symmetries of the energy levels in the gap), these studies lacked the required precision to provide reliable electrical levels to be compared with the experimental data. They also provided some initial estimates for migration barriers [15], but the neglect of structural-relaxation effects undermine any tentative connection to the experiments. More recently, light 3d-row TM impurities in Si have been subjected to the scrutiny of *state-of-the-art* DFT calculations using transferable pseudopotentials, and including fully structural relaxation effects in periodic supercells [20–24]. Unfortunately, with the exception of Ti [23],

*marinop@ua.pt

only neutral states were considered [21]. Further, the reported barriers exhibited strong discrepancies with the available diffusivity data, maybe reflecting the fact that the corresponding calculations were performed on rather small (sixteen-atom) supercells [20]. Interestingly, Estreicher and co-workers [25] have shown that the calculated barriers of point defects that are strongly bound to the lattice (such as interstitial oxygen) can show error bars above 0.1 eV, while the barriers of lightly bond defects (such as interstitial iron) usually show much lower discrepancies with respect to the experiments.

Among the above mentioned first-principles studies, exchange and correlation was described within the local density (LDA) or semilocal generalized-gradient (GGA) approximations, whose suitability for strongly correlated problems is questionable and prone to self-interaction errors [26]. The self-interaction error manifests itself to an unphysical curvature of the total energy with respect to fractional electron occupations. In contrast, an exact DFT functional would lead to a piecewise linear dependence of the energy between integer values of electron occupancies [26,27]. One way to include on-site correlation effects within DFT is by means of the DFT+U approach. This is a semiempirical method initially introduced as a Hubbard-corrected local density approximation (LDA+U) by Anisimov and co-workers [28], who extended the standard LDA functional with a Hubbard-type correction that contains an intra-atomic electron Coulomb interaction U acting exclusively on the subset of highly correlated electrons. LDA+U has been very successful in the description of insulating TM oxides bringing band gaps and other observables such as magnetic moments into much better agreement with the experiments. On-site exchange effects were also added via a screened exchange parameter J [1]. However, U and J are system-dependent quantities and there is no obvious way to obtain them. Many DFT+U studies include a preliminary step where U and J values are varied in order to reproduce experimentally measured quantities such as the electronic band gap [29]. However, this common practice challenges the unbiased nature of the underlying first-principles calculations.

In the present work, we employ both standard DFT and the rotationally invariant DFT+U formulation of Liechtenstein *et al.* [30] to calculate the electrical levels and migration barriers of six early 3d and 4d TM impurities in silicon, namely, Ti, V, Cr, Zr, Nb, and Mo. In this specific DFT+U scheme, the on-site U and J parameters enter separately (as opposed to alternative methodologies [7,31] where on-site correlation is accounted for through the effective interaction $U - J$), providing a flexible and clear assessment of Coulomb and exchange effects. The parameter J, in particular, describes intra-atomic exchange effects: it is a measure of Hund's coupling whereby mutually aligned spins preferentially occupy empty single-particle states on the same site, therefore maximizing the total spin S. The existence of defect states in the gap with a multitude of electron occupancies [17,19,32] can give rise to very different spin states with distinct J values. A recent study [33] demonstrated the importance of the intra-atomic exchange J to the description of magnetic susceptibilities and magnetoelectric response of noncollinear antiferromagnetic materials. In the present work, the on-site Hubbard U and Hund's J parameters are not treated as adjustable constants. Instead, they are determined self-consistently from linear-response theory and constrained DFT calculations [26,34] that take into account the local environment of the impurity [35] and reduce the residual self-interaction error.

The paper is divided as follows. In Sec. II, we introduce the theoretical framework for the total energy calculations, including a description of the calculation of U and J parameters. In Sec. III, we start by reporting the results of the U and J values for all six TMs under scrutiny. We also present the results on their electrical levels and migration barriers, comparing with the existing experimental data and discussing the impact of correlation and exchange effects. Finally, we close the paper in Sec. IV with the concluding remarks.

II. THEORETICAL FRAMEWORK

Density-functional calculations (ground-state atomic and electronic structures, electrical levels and migration barriers) were carried out using the VASP code [36–38] and were based on the projector augmented-wave method [39,40]. The exchange-correlation potential was accounted for within the GGA through the use of the Perdew-Burke-Ernzerhof (PBE) functional [41]. Semicore 3s and 3p (4s and 4p) states of the 3d-row (4d-row) transition metals were described explicitly as part of the valence shells. The Kohn-Sham states were expanded in plane waves with a kinetic energy cutoff $E_{\rm cut} =$ 300 eV. Such a cutoff energy was found sufficiently high to provide converged energy differences within a tolerance of 5 meV. For the defect calculations, large 512 Si-atom cubic supercells were employed. These were constructed from a fourfold replication of the conventional eight-atom cubic cell along each principal direction with a theoretical lattice parameter $a_0 = 5.465$ Å. The final results included full structural and electronic/spin relaxations with L-point sampled Brillouin-zones. Our choice of the L point to sample the Brillouin zone is itself an approximation and was based on (i) the fact that we are using a large supercell, (ii) the high symmetry of this $\mathbf{k}$ point, which like Γ captures the full symmetry of the problem, allowing us to inspect possible Jahn-Teller effects in a clearer way, and (iii) the wider direct gap at this point in the Kohn-Sham band structure, which to some extent, mitigates the underestimated indirect gap due to a nonexact treatment of the exchange-correlation interactions. Consequently, gap states at the L point are less affected by overmixing with crystalline states of the host. A smearing width of 0.002 eV was used for filling in electronic states near the Fermi energy.

Both conventional DFT and DFT+U approaches were employed on the present defect studies. In the latter case, the rotationally invariant formulation of DFT+U originally introduced by Liechtenstein and co-workers [30] was adopted. Accordingly, the total energy functional of the electron σ-spin density $n^\sigma(\mathbf{r})$ is recast as

$$E_{\rm DFT+U}[n^\sigma(\mathbf{r}),\mathbf{n}^{I\sigma}] = E_{\rm DFT}[n^\sigma(\mathbf{r})] + E^{U,J}_{\rm Hub}[\mathbf{n}^{I\sigma}] - E^{U,J}_{\rm dc}[\mathbf{n}^{I\sigma}], \quad (1)$$

where $E_{\rm DFT}$ is the usual DFT total-energy functional and $E^{U,J}_{\rm Hub}$ is a Hubbard-type corrective functional operating exclusively on strongly correlated states (*ex.* states with

angular momentum $l = 2$ or $l = 3$ in transition metals or lanthanides, respectively) that depends on a $\mathbf{n}^{I\sigma} \equiv \{n^{I\sigma}_{mm'}\}$ $2l+1$-fold occupation matrix. Superscripts U and J emphasize a parametric dependence on screened Coulomb and exchange constants. The $n^{I\sigma}_{mm'}$ elements are constructed from site projections of the Kohn-Sham states $\psi^{\sigma}_{\mathbf{k},\lambda}$ (here labeled by a wave-vector/band-index pair, $\mathbf{k},\lambda$) onto atomiclike orbitals ϕ^{I}_{m} located on site I with a magnetic quantum number m. Hence $n^{I\sigma}_{mm'} = \sum_{\mathbf{k},\lambda} f^{\sigma}_{\mathbf{k},\lambda} \langle \psi^{\sigma}_{\mathbf{k},\lambda} | P^{I}_{mm'} | \psi^{\sigma}_{\mathbf{k},\lambda} \rangle$, where $f^{\sigma}_{\mathbf{k},\lambda}$ is an occupation number and $P^{I}_{mm'} = |\phi^{I}_{m}\rangle\langle\phi^{I}_{m'}|$ is a generalized projection operator (see, for example, Ref. [26] for further details). $E^{U,J}_{\mathrm{dc}}$ is an additional correction to avoid double-counting of interactions among the correlated electrons [28].

The on-site U and J parameters for each TM were calculated separately by means of a linear-response procedure as proposed by Cococcioni and coworkers [26,34]. This particular set of calculations was carried out using the QUANTUM ESPRESSO package [42] considering defect configurations that were previously relaxed using the VASP code. Again, the underlying exchange and correlation potential was accounted for by the GGA through the use of the Perdew-Burke-Ernzerhof (PBE) functional [41]. Valence-core interactions were described by means of ultrasoft pseudopotentials [43] and a plane-wave basis cutoff was set at 300 eV and 1200 eV for the expansion of the Kohn-Sham states and charge density, respectively. We found these values adequate to provide an acceptable convergence for the Hubbard parameters. The effect of increasing these cutoffs up to 400 and 4000 eV led to maximum deviations of 0.20 eV for the U and J parameters.

The procedure for the calculation of the U parameter starts from the self-consistent density of the DFT ground state of an impurity in a supercell. The basic idea is to obtain numerically the total-energy curvature with respect to variations of the d-electron occupancies and recover the exact piecewise linear dependence [26]. This problem can be recast into linear-response calculations where the U values satisfy the above requirement and are obtained from the density-response functions after imposing local perturbations to the TM sites I. These perturbations consist of potential shifts α_I of magnitude up to 0.05 eV. Next, one calculates the total on-site d-electron occupation $n_I = \sum_{\sigma,m} n^{I\sigma}_{mm}$ before and at the end of electronic self-consistency cycle, resulting in noninteracting (χ^{0}_{I}) and screened (χ^{scr}_{I}) on-site response functions defined as

$$\chi^{0}_{I} = \frac{\Delta n^{0}_{I}}{\Delta \alpha_I}, \quad \chi^{\mathrm{scr}}_{I} = \frac{\Delta n^{\mathrm{scr}}_{I}}{\Delta \alpha_I},$$

and the on-site parameter U is finally obtained from

$$U = \left(\chi^{0}_{I}\right)^{-1} - \left(\chi^{\mathrm{scr}}_{I}\right)^{-1}. \tag{2}$$

In a similar manner, Hund's exchange parameters J for the TMs were determined from the self-consistent response of on-site magnetizations $m_I = n^{\uparrow}_{I} - n^{\downarrow}_{I}$ to on-site perturbations $\beta_I m_I$ (with β_I values up to ± 0.05 eV) imposed on the TM sites (see Ref. [34] for further details). In this case, however, we used the DFT+U ground states as the noninteracting reference configurations to which perturbations were applied.

Electrical levels of impurities were determined by means of the marker method [44]. This approach is based on a comparison between electron affinities (A) or ionization energies (I) of a particular defect under scrutiny, with analogous A and I's calculated for a reference system (referred to as *marker*). Unfortunately, in the absence of vacuum space, such as in the limit of an infinite solid within periodic boundary conditions, absolute values of A and I are ill-defined. Additional difficulties arise in the calculation of A and I using periodic supercells, where spurious effects such as (i) electronic dispersion of defect levels, (ii) elastic strain, or (iii) long-ranged electrostatic interactions built up on a lattice of charged defects pose complications to the accuracy of the predictions.

The marker method is claimed to remove, or at least to mitigate, some of these difficulties, including the nonexact treatment of the exchange-correlation interactions through cancellation of terms at the expense of bringing in an empirical correction [44,45]. Accordingly, a donor-transition level with respect to the valence-band (VB) edge, E_{V}, is given by

$$E_{\mathrm{D}}(q/q+1) - E_{\mathrm{V}} = I_{\mathrm{D}}(q/q+1) - I_{\mathrm{M}}(q/q+1) + \{E_{\mathrm{M}}(q/q+1) - E_{\mathrm{V}}\}_{\mathrm{exp}}, \tag{3}$$

where the I values are calculated from first-principles, while the third term on the right (between curly brackets) is an experimental quantity and refers to the donor level of the marker defect with respect to E_{V}. Subscripts D and M stand for the *defect* being examined and *marker*, respectively. Finally, the ionization energies are

$$I(q/q+1) = E(q) - E(q+1) + \xi(q) - \xi(q+1),$$

where $E(q)$ is the total energy of a defective supercell in charge state q, and $\xi(q)$ is a correction bundle incorporating all the above mentioned sources of errors for each charge state. The strength of the method lies on the hypothesis that $\xi_{\mathrm{D}}(q) - \xi_{\mathrm{D}}(q+1) \approx \xi_{\mathrm{M}}(q) - \xi_{\mathrm{M}}(q+1)$ so that these corrections mutually cancel in the calculation of $I_{\mathrm{D}} - I_{\mathrm{M}}$ in Eq. (3). This is usually true when the defect under study and the marker have gap states with similar shape (symmetry and localization). We note that Eq. (3) does not involve the calculation of a band gap or a band edge. Donor (acceptor) levels of defects are simply calculated with respect to donor (acceptor) levels of a particular marker. Unfortunately, many defects have no particularly suitable marker and the use of a proper first-principles approach is highly desirable. As proposed by Jeong and Oshiyama [46], we may assume that our marker is a bulk supercell corresponding to $E_{\mathrm{bulk}}(q/q+1) - E_{\mathrm{V}} = 0$, and Eq. (3) simply becomes

$$E_{\mathrm{D}}(q/q+1) - E_{\mathrm{V}} = I_{\mathrm{D}}(q/q+1) - I_{\mathrm{bulk}}(q/q+1). \tag{4}$$

Although well grounded for donor (acceptor) levels with a strong admixing degree with crystalline valence-band (conduction-band) states, the applicability of Eq. (4) to defects with strongly localized midgap states could be questionable. Equation (4) involves the calculation of the valence-band top energy (assumed to be I_{bulk}), which can be erroneous when using (semi)local DFT functionals. This problem has been recently raised by Alkauskas, Broqvist and Pasquarello [5], who showed that a proper alignment of the band edges with respect to the average electrostatic potential significantly improves the calculated levels, bringing them to a better agreement with the experiments. It was also clear that this

improvement was more significant for materials with severely underestimated band gaps (such as metal oxides). Although our calculations using the bulk marker [Eq. (4)] are certainly affected by such errors, we expect them to be relatively small in silicon, particularly for the case of defect-marked levels [Eq. (3)]. Further, the marker method has been a longstanding and successful approach to predict defect levels in group-IV semiconductors [45,47–50].

Considering the size of the supercells employed in this work and the localization of the electronic states of interest, artificial electrostatic errors from charged calculations are likely to dominate the correction to $I_{\rm D}(q/q+1)$. To first order, this can be approximated by the so-called Madelung correction [51]:

$$\xi_{\rm D}(q) - \xi_{\rm D}(q+1) \approx -\frac{\alpha_{\rm M}}{\epsilon L}(2q+1),$$

where $\alpha_{\rm M}$ is the Madelung constant of the supercell with characteristic length L ($\alpha_{\rm M} = 1.41866$ and $L = 21.86$ Å for a 512-Si atom cubic supercell), and $\epsilon = 11.4$ is the static dielectric constant of silicon.

On the other hand, the Madelung correction is expected to be hardly applicable to $I_{\rm bulk}(q/q+1)$ [52]. Such calculation involves ionizing the top-most occupied crystalline state, which produces a positive charge density spanning the whole cell, along with a compensating background negative density to maintain charge neutrality. A more suitable charge correction for this case would be the electrostatic energy of *jellium*, which turns out to vanish due to long-range cancelation of the electronic, background and electron-background interactions [53]. Hence we assume that $\xi_{\rm bulk}(q) - \xi_{\rm bulk}(q+1) \approx 0$ and a donor level with respect to the valence band top is finally obtained as

$$E_{\rm D}(q/q+1) - E_{\rm V} = I_{\rm D}(q/q+1) - I_{\rm bulk}(q/q+1) - \frac{\alpha_{\rm M}}{\epsilon L}(2q+1). \quad (5)$$

Similar arguments are applicable for acceptor levels, although in this case we should be comparing electron affinities.

III. RESULTS

Initial DFT calculations provided the minimum-energy ground states of all TMs occupying the tetrahedral interstitial positions in the silicon lattice. Structural relaxations were performed for charge states ranging from double plus to single minus. The respective electronic spin states S were also found by concurrently minimizing the energy with respect to spin polarization. Several low-symmetry structures away from the perfect tetrahedral symmetry of the interstitial site were considered. This was done in order to avoid structural trapping at symmetry-constrained Jahn-Teller (JT) instabilities. The resulting electronic structure of the interstitial TMs was qualitatively similar to earlier first-principles results for the $3d$-row [17,19] and $4d$-row metals [18], respectively. Regarding the effect of structural distortions away from the perfect tetrahedral symmetry, significant energy lowering was obtained for specific JT distortions mainly within DFT+U. In this case, the most prominent energy gains took place for the following metals (magnitude of energy lowering in meV and corresponding symmetry of the distortion given inside parentheses): ^{1}Ti^{++} (262, C_{3v}), $^{1/2}$V^{0} (351, C_{2v}), ^{1}V^{+} (87, C_{3v}), ^{1}Zr^{++} (85, C_{2v}), $^{1/2}$Nb^{0} (98, C_{3v}), ^{1}Nb^{+} (104, C_{3v}), and $^{1/2}$Mo^{+}(196, C_{3v}), where spin and charge states are left- and right-superscripted to each species, respectively. In contrast, distortions from the ideal tetrahedral symmetry had a much smaller impact within DFT with the largest energy lowering found for $^{1/2}$V^{0} (67, C_{3v}) and ^{1}V^{+} (67, C_{3v}). We point out that Born-Oppenheimer approximated DFT (which overlooks electron-phonon interactions) is fundamentally unsuitable to the treatment of the Jahn-Teller effect. In that respect, the above values should be considered with due caution.

In agreement with Ludwig and Woodbury [32], we found that the d-electron atomic levels split into triplet (t_2) and doublet (e) states when the TM atom is inside the solid. While the atomic configurations of $3d$ ($4d$)-row elements have fully occupied $4s$ ($5s$) states, in silicon these states resonate with the conduction band (CB) and, therefore, their electrons drop to the lowest unoccupied $t_2 + e$ manifold in the gap. For instance, Ti with a [Ar] $3d^2\ 4s^2$ atomic configuration, when inserted at the tetrahedral interstitial site of silicon shows a $3d^4\ 4s^0$ electron configuration, or more precisely $(t_2^4 + e^0)\, a_1^0$ using a representation within the T_d symmetry point group. For all six TMs, the t_2 state was always found lower in energy with respect to e and therefore it is preferentially occupied. Furthermore, while t_2 was always calculated inside the gap (see Fig. 1), with the exception of V and Cr species, the e state appeared as a resonance within the CB.

As expected, we found that DFT+U tends to increase the gap between occupied and unoccupied states in the defective supercells. For the sake of example, Fig. 1 compares band

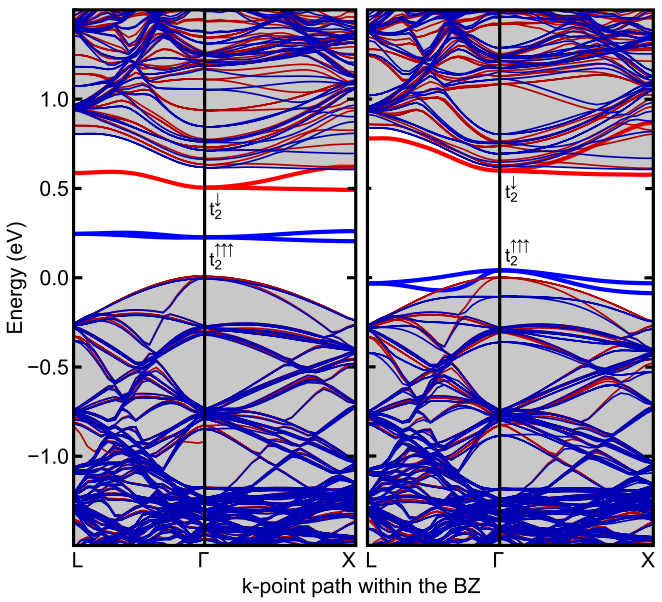

FIG. 1. (Color online) Band structure of an interstitial ^{1}Ti^{0} impurity in silicon obtained within spin-polarized DFT (left) and DFT+U (right). In the latter case U and J were equal to 4.6 and 0.6 eV, respectively. The electron occupations of the spin-up and spin-down channels of the triplet (t_2) are denoted by the arrows. Blue (red) curves denote the spin-up (spin-down) electron states. Shaded regions denote bulklike host states. The valence-band maximum defines the zero energy.

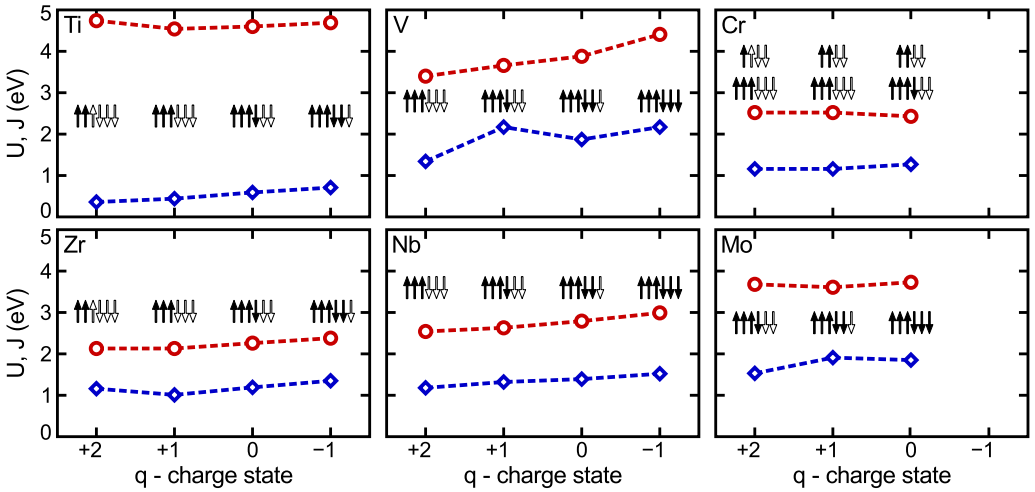

FIG. 2. (Color online) Magnitude of the on-site Hubbard U and Hund J parameters of single interstitial TMs in silicon obtained as a function of their charge/spin state. The electron occupancies from DFT calculations for both spin channels of the triplet (t_2) are depicted as arrows with filled (empty) symbols denoting the occupied (unoccupied) electron states. The doublet state is always empty, except for Cr, where the occupancies of the doublet (e) are also shown explicitly.

structures obtained from DFT (on the left) and from DFT+U calculations (on the right) for a 512-Si atom supercell with a neutral Ti impurity at the tetrahedral interstitial site. Within DFT, the triplet state t_2 is seen to lie deep in the gap with a small (although noticeable) dispersion along the chosen Brillouin zone (BZ) path. The t_2 spin-up channel has an occupation of three electrons, whereas the corresponding spin-down channel accommodates one electron to make a net $S = 1$ state. The highest degeneracy (symmetry) of the electronic structure holds at Γ and L points of the Brillouin zone. Within DFT+U the splitting of the two t_2 spin channels is amplified and close to the center of the zone they mix considerably with the bulk crystalline density of states. We found that this effect is smaller at $\mathbf{k} = L$, i.e., where the direct Kohn-Sham gap is wider (1.21 eV). We also note that this is the $\mathbf{k}$-point used to build the electron density, $n(\mathbf{r}) = \sum_{\lambda,\sigma} f^{\sigma}_{\mathbf{k}=L,\lambda} |\psi^{\sigma}_{\mathbf{k}=L,\lambda}(\mathbf{r})|^2$, and respective potential and total energy.

Figure 2 depicts the calculated ground-state occupancy of the t_2 level ($t_2 + e$ levels for Cr) for all TMs considered for several charge states. These results were obtained after inspection of the Kohn-Sham states at $\mathbf{k} = L$. Triplets and doublets are represented by sixfold and fourfold sets of arrows, respectively, where the occupancy of each component is indicated by filling in the respective arrow. In general, the resulting ground state for each TM impurity was obtained from the sole occupation of the t_2 state. For V and Cr, where the doublet falls into the gap, we also considered configurations that resulted from the occupation of the $t_2 + e$ manifold. Cr in particular is a borderline case within DFT as also evidenced in previous first-principles calculations [17]. Accordingly the $^2\mathrm{Cr}^0$ high-spin (HS) state (shown in Fig. 2) was nearly degenerate to the $^0\mathrm{Cr}^0$ LS state. The latter has electron occupancies analogous to Mo (see Fig. 2). The present DFT results show that the neutral HS configuration of Cr is favored with respect to the neutral LS one by 0.06 eV. Similarly, HS Cr is energetically more favorable for the other charge states as well, with the largest energy difference attained for the singly-positive charge, Cr^+ (0.43 eV). V is also a borderline case. Within DFT, the neutral low-spin $^{1/2}\mathrm{V}^0$ ground state is slightly more stable (by 0.19 eV) when compared to the high-spin $^{5/2}\mathrm{V}^0$ state. Analogously, V^+ preferably adopts a LS $S = 1$ state, as depicted in Fig. 2. Within DFT+U the LS state $^{1/2}\mathrm{V}^0$ of V^0 is also favored. However, now the HS state ($S = 2$) of V^+ is lower in energy with respect to the LS $S = 1$ state (by 0.14 eV). The existing observations of the EPR-active charge states of the 3d-row metals are in agreement with the present findings. In particular, EPR experiments [10,11,54] established the following charge/spin states: Ti^+, V^{++}, and Cr^+ with electron spin S equal to 3/2, 3/2 and 5/2, respectively, matching the results reported in Fig. 2.

The calculations of the Hubbard U and J parameters were carried out using the fully relaxed TM configurations from DFT as previously outlined. As an example, Fig. 3 shows the calculated d-state occupation and magnetization of a neutral Ti impurity in Si as a function of local perturbations to the on-site potential. Response functions χ^0_I and χ^{scr}_I were obtained from the slopes of the noninteracting and screened response lines, respectively (shown up in Fig. 3 as dashed and solid lines, respectively).

The obtained values of the U and J parameters for the six TMs in their respective ground states are shown as circles and diamonds in Fig. 2, respectively. The same figure also depicts the resulting spin configurations and the detailed spin-up and spin-down electron occupancies for each charge state. The magnitude of the U parameters is seen to be in the 2-5 eV range whereas J attains values of up to about 2 eV (the larger J values are found for certain charge states of V and Mo). It is difficult to draw conclusive statements about the calculated trends of U and J since several factors beyond the electronic and spin occupation ordering affect the final results. These include structural relaxation effects, the position of the t_2 levels within the gap and mixing degree with the host density of states. In general, our calculations show that U and J increase slightly as electrons are added to the d-like states of the TM impurities. For the Ti/Zr and V/Nb groups,

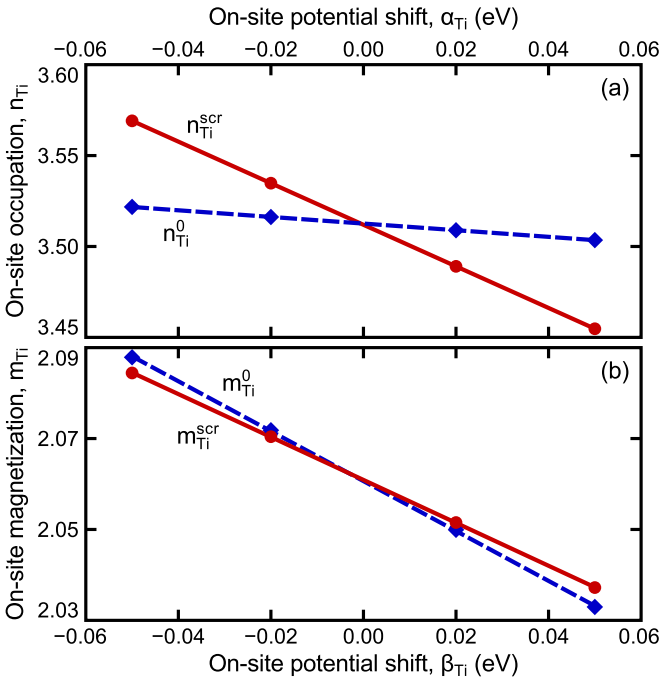

FIG. 3. (Color online) Noninteracting (diamonds) and screened (circles) on-site occupation (a) and magnetization (b) as a function of a local perturbation to the potential on d electrons of a neutral Ti interstitial impurity in silicon. Dashed and solid lines represent the best linear fit to the data, from which χ^{0}_{Ti} and χ^{scr}_{Ti} were obtained, respectively.

the half-filled configuration of t_2 (three electrons of parallel spin) leads to the lowest values of U. On the other hand, J takes its largest values for the negatively-charged state of each metal. This is consistent with earlier interpretations [34] where the positive J term in the effective interaction penalizes configurations with antiparallel spins on the same site. The magnitude of U is generally higher for the 3d TMs than for their 4d counterparts, reflecting a weaker screening and the more delocalized character of the 4d orbitals. This, however, does not hold for Cr, where unlike for Mo the e-state drops into the gap, and shares the available d-like electrons with the t_2 state. To appraise the effect of eventual Jahn-Teller distortions to the final values of U and J, further test calculations using unrelaxed supercells with the TMs occupying the interstitial tetrahedral sites were also carried out. The results showed rather small changes of both U and J, with deviations of up to 0.15 and 0.25 eV, respectively.

Table I lists the U and J parameters for all six metals in their respective neutral ground states. These parameters were subsequently used to determine the electrical levels of the six TMs within DFT+U. Both U and J are not variational with respect to the density. Hence, $E(q/q+1)$ becomes ill-defined when obtained using different Hubbard and Hund parameters (for instance if calculated for their respective q and $q+1$ charge states). This poses a difficulty in the determination of electrical levels within DFT+U. In the present work, we assumed fixed U and J's, being equal to the ones for the neutral states of the respective metals. We further performed a number of test calculations of the levels, $E(q/q+1)$, in particular by averaging the U and J parameters over the two charge states q and $q+1$ involved in the transition. The results turned out to be very similar with the largest discrepancy amounting to 0.03 eV.

TABLE I. Calculated U and J values of the six early 3d and 4d TMs in silicon (all values in eV). The results refer to the neutral DFT ground state of each metal (with corresponding spin values S shown as left superscripts on the species symbol). The electron occupancies of the spin-up and spin-down channels are also shown as arrows.

TM	State	U	J
$^{1}Ti^{0}$	$t_2^{\uparrow\uparrow\uparrow\downarrow}e^{0}$	4.6	0.6
$^{1/2}V^{0}$	$t_2^{\uparrow\uparrow\uparrow\downarrow\downarrow}e^{0}$	3.9	1.9
$^{2}Cr^{0}$	$t_2^{\uparrow\uparrow\uparrow\downarrow}e^{\uparrow\uparrow}$	2.4	1.3
$^{1}Zr^{0}$	$t_2^{\uparrow\uparrow\uparrow\downarrow}e^{0}$	2.3	1.2
$^{1/2}Nb^{0}$	$t_2^{\uparrow\uparrow\uparrow\downarrow\downarrow}e^{0}$	2.8	1.4
$^{0}Mo^{0}$	$t_2^{\uparrow\uparrow\uparrow\downarrow\downarrow\downarrow}e^{0}$	3.7	1.9

A. Electrical levels

The calculated electrical levels for the six metals, obtained by both DFT and DFT+U, are listed in Table II together with the corresponding experimental results. Additionally, a graphical representation of the levels is depicted in Fig. 4, where their positioning with respect to the band edges of bulk silicon is reproduced from the calculations. In Fig. 4, we assume that the band gap $E_C - E_V$ is the experimental value, 1.17 eV. This is actually very close to the theoretical one, if we consider the quasiparticle gap as $A - I = E(+) + E(-) - 2E(0) = 1.21$ eV, obtained using 512-Si atom supercells with the BZ sampled at $\mathbf{k} = L$. We note that this assumption is not related to a scissorslike operation—all donor (acceptor) levels are calculated with respect to E_V (E_C). Similarly in Table II, all levels are referred with respect to the band edges without involving the band gap. The levels were determined using two different markers: first, the bulk Si crystal and secondly the Ti interstitial defect for which the existing experimental electrical levels are well established. The corresponding results are reported in Table II inside and outside parentheses, respectively, for both markers. The levels are also depicted in Fig. 4 for the former marker.

For the sake of example, we briefly describe the calculation of Ti(0/+) and Mo(0/+) levels within DFT+U. The ionization energies (calculated from total energies with the BZ sampled at L) of interstitial Ti and Mo ions in a 512 Si atom supercell are $I_{Ti}(0/+) = 6.33$ eV and $I_{Mo}(0/+) = 5.80$ eV. These are 0.98 and 0.45 eV *above* the ionization energy of bulk [$I_{bulk}(0/+) = 5.35$ eV], which is the marker. This places the first donor levels of Ti and Mo at $E_V + 0.98$ eV and $E_V + 0.45$ eV, respectively. An alternative perspective can be achieved by considering Ti as the marker, and comparing directly $I_{Ti}(0/+)$ with $I_{Mo}(0/+)$. From the values above, we have that $I_{Ti}(0/+)$ is located 0.53 eV above $I_{Mo}(0/+)$. According to the marker method and considering that Ti(0/+) has been experimentally established at $E_V + 0.87$ eV, we predict that Mo(0/+) is located at $E_V + 0.87 - 0.53 = E_V + 0.34$ eV. This is to be compared

TABLE II. Calculated (DFT and DFT + U) and experimental (Exp.) electrical levels of the early 3d and 4d TMs in silicon (values in eV). The theoretical results were obtained by taking two different marker choices: the bulk Si crystal and the Ti interstitial defect (the results from the latter method are shown within parentheses).

	Ti			V			Cr		
3d row	DFT	DFT+U	Exp.[a]	DFT	DFT+U	Exp.[b]	DFT	DFT+U	Exp.[c]
$E_C - E(-/0)$	0.21	0.05	0.09	0.34 (0.22)	0.01 (0.06)	0.20	0.18 (0.06)	0.11 (0.16)	–
$E_V + E(0/+)$	0.78	0.98	0.87	0.62 (0.71)	0.86 (0.75)	0.72	0.78 (0.87)	0.86 (0.75)	0.94
$E_V + E(+/++)$	0.17	0.23	0.26	0.34 (0.43)	0.30 (0.33)	0.34	– (–)	– (–)	–
4d row		Zr			Nb			Mo	
	DFT	DFT+U	Exp.[d]	DFT	DFT+U	Exp.	DFT	DFT+U	Exp.
$E_C - E(-/0)$	0.27 (0.14)	0.23 (0.28)	0.14	0.41 (0.29)	0.34 (0.39)	0.32[e], 0.293[f]	– (–)	– (–)	0.27[g]
$E_V + E(0/+)$	0.71 (0.80)	0.74 (0.63)	0.76	0.51 (0.60)	0.56 (0.45)	0.57[e], 0.59[f]	0.31 (0.40)	0.45 (0.34)	0.30[h]
$E_V + E(+/++)$	0.28 (0.37)	0.29 (0.32)	0.32	0.20 (0.29)	0.25 (0.28)	0.21[e], 0.163[f]	0.01 (0.10)	0.00 (0.03)	–

[a]Reference [64].
[b]Reference [58].
[c]Reference [60].
[d]Reference [12].
[e]Reference [13].
[f]Reference [66].
[g]References [56,65].
[h]References [55–57].

with a measurement that suggests that Mo(0/+) lies at E_V + 0.3 eV [55–57].

It can be seen in Table II that in most cases, the agreement between the experimental data and both DFT and DFT+U calculations is very good, with differences between theory and experiment not exceeding ∼0.1 eV. A comparison between the DFT and DFT+U results shows that the effect of on-site correlation is considerably more pronounced for the 3d metals, in particular for Ti and V. These are the species with the larger on-site U parameters, suggesting that Coulomb effects are

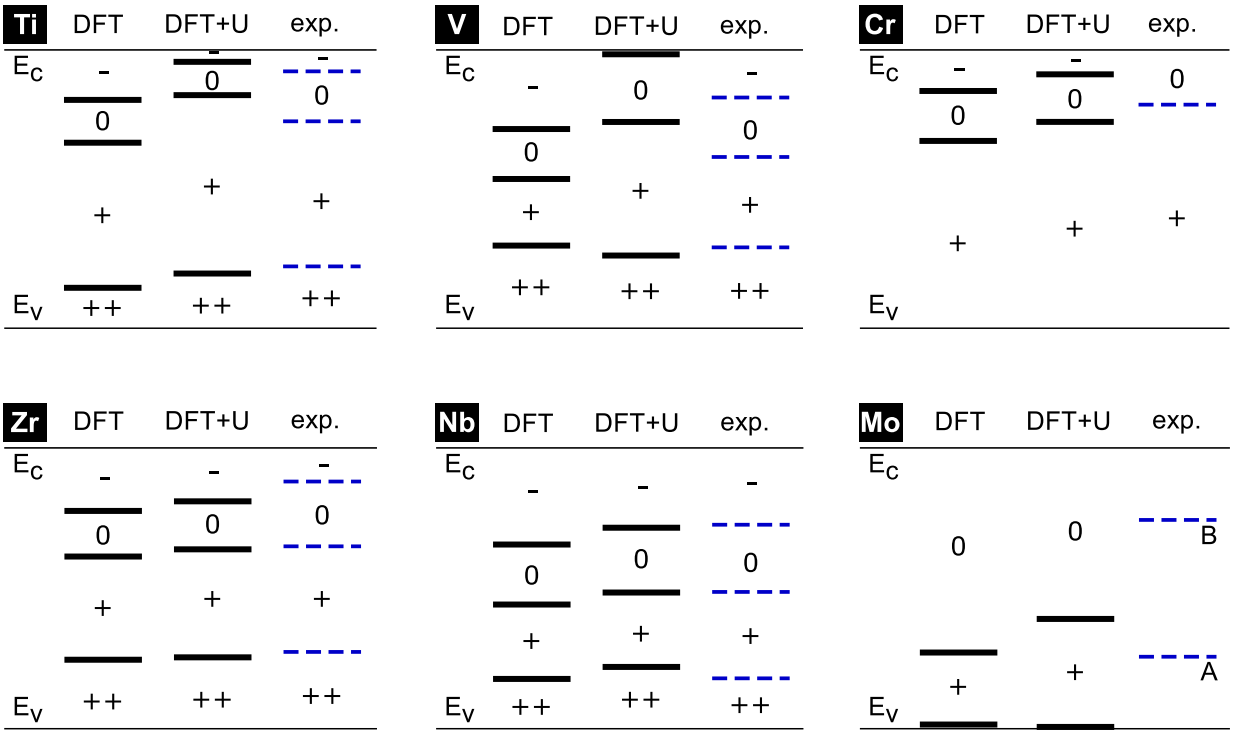

FIG. 4. (Color online) Graphical representation of the electrical levels of the six early 3d and 4d TMs in silicon from DFT and DFT+U calculations. The results were obtained by taking as marker the bulk Si crystal. The valence-band and conduction-band edges of silicon are denoted by E_V and E_C, respectively. The experimental levels are taken from the following works: Ref. [64] for Ti, Ref. [58] for V, Refs. [60,63] for Cr, Ref. [12] for Zr, Ref. [13] for Nb, and Ref. [55] for Mo. Charge states of Mo levels are still a matter of debate and they are denoted by A and B transitions (see text).

more important for these species. By examining the position of the electrical levels in the gap (see Fig. 4) it can be inferred that DFT+U tends to shift the DFT levels towards higher energies. This effect arises from the accumulated correlation energy (underestimated in standard DFT) as we add electrons to the TM d shell. This is particularly noticeable for the acceptor and single-donor levels of the 3d-row metals. For Ti, the shift in all its three levels improves the overall agreement with the reported experimental data (see Table II and Fig. 4). The most dramatic manifestation is for V where its acceptor level, V(−/0), becomes almost resonant with the conduction band. This result represents the largest discrepancy of the present calculations with the existing experimental data: the experimental evidence points out to a stable and deeper V(−/0) level around $E_C - 0.2$ eV [9,58]. The acceptor level determined by DFT is even deeper ($E_C - 0.34$ eV), placing the experimental data about midway between the DFT and DFT+U results.

For the case of Cr the well established Cr(0/+) donor level is well reproduced by both DFT and DFT+U in the upper part of the gap (see Fig. 4). Also, we did not obtain a double-donor level, Cr(+/++), inside the gap by either DFT or DFT+U. This finding agrees with the work of Feichtinger and Szaputa [59], who combined EPR with Hall-effect measurements. While some further investigations [60] did not confirm the presence of a stable double-donor level for Cr, other experimental studies [61–63] have reported a Cr(+/++) level within a range from $E_V + 0.11$ eV to $E_V + 0.31$ eV. These particular observations seem to be in line with previous calculations [16,17] that predict rather deep Cr(+/++) levels at $E_V + 0.35$ eV and at $E_V + 0.55$ eV. Our results suggest that the origin of these levels is probably due to other defect complexes involving Cr. In particular, Cr-B pair complexes in p-type silicon may give rise to such levels in the lower part of the gap [60]. Finally, our DFT and DFT+U calculations for Cr predict an acceptor level inside the gap, which to our knowledge has not been observed experimentally.

For the 4d metals, the differences among DFT and DFT+U results are modest and appear to scale with the magnitude of the effective interaction which is commonly defined as $U - J$ (see Fig. 4) [31]. For Zr (which possesses the smallest $U - J$ value of about 1 eV), the largest deviation between DFT and DFT+U takes place for its acceptor level, which shifts slightly (only by 0.06 eV) closer to the CB edge. For Zr and Nb, which introduce three deep levels inside the gap, the theoretical results reproduce with very good accuracy the experimental data. For Mo, on the other hand, both DFT and DFT+U predict only one deep level of single-donor character. DFT+U places this level at $E_V + 0.45$ eV, a bit deeper in the gap (by about 0.14 eV) with respect to the DFT prediction. This shift is consistent with the larger $U - J$ value (of about 2 eV) for Mo. Experimentally, for this metal, most existing studies [9,55,57] report a donorlike level at about $E_V + 0.30$ eV (denoted as A in Fig. 4), without, however, specifying whether it is the double-donor or the single-donor level of Mo. Our results clearly suggest that this level is the Mo(0/+) level rather than a double-donor transition. The latter, instead, is found to be virtually resonant with the VB top by either DFT or DFT+U. Furthermore, the present results show that no acceptor level can be expected inside the gap for interstitial Mo in silicon. Experimentally, the existence of additional deep levels for Mo (above the Mo(0/+) level at $E_V + 0.30$ eV) was reported in two studies which, however, place them closer to the CB edge with some further controversy regarding their nature and origin. Hamaguchi and Hayamizu [56] connected at least two prominent deep levels to Mo defects at $E_C - 0.34$ eV and $E_C - 0.27$ eV. Finally, Cox [65] reported an acceptorlike level at $E_C - 0.269$ eV (denoted as B in Fig. 4), which was ascribed to substitutional rather than interstitial Mo. Given that both our DFT and DFT+U results do not predict a stable acceptor level for interstitial Mo inside the gap, our view is that the acceptor level reported by Cox [65] could indeed originate from substitutional Mo, or perhaps from the interaction between interstitial Mo with an unavoidable impurity such as hydrogen. Further calculations, however, are needed to fully clarify this point.

It is clear from the discussion above that certain theoretical results require further confirmation. In particular, (a) for V, the position of the acceptor level, V(−/0), determined from DFT+U is found extremely close to the CB edge ($E_C - 0.01$ eV), either suggesting an unstable acceptor state, or the overestimation of correlation within the d electrons. Most of the existing experimental studies [9,58] report an acceptor level for interstitial V at $E_C - 0.16$ eV [9] or at $E_C - 0.20$ eV [58]. (b) For Cr, the existence of a double-donor level, Cr(+/++), inside the gap. (c) Confirmation that indeed the widely-observed level assigned to Mo at $E_V + 0.30$ eV is of single-donor type. In order to appraise the above issues and introduce a better level of confidence, we further determined the electrical levels using a different marker. To this end, the Ti interstitial defect was chosen as an alternative marker, for which the calculated levels (by considering as marker the bulk Si crystal) are in very good agreement with the experiments for both DFT and DFT+U (see Fig. 4). The calculated levels with the Ti marker are also listed in Table II, inside parentheses. The DFT+U result for V(−/0) is now improved with the level lying deeper in the gap ($E_C - 0.06$ eV), closer to the experimentally observed level [9]. Additionally, considerable improvement is obtained for V(0/+) and V(+/++). Concerning Cr the calculations with the Ti marker confirm the previous results—no double-donor level was found in the gap. For Mo, the Ti-marked calculations again show that it is the single-donor level, Mo(0/+), that matches well the widely-reported level at $E_V + 0.30$ eV. In fact, the DFT+U result at $E_V + 0.34$ eV for Mo(0/+) agrees now much better with the experimental data. Similarly to the results using the bulk-Si marker, we did not obtain further deep levels in the gap for Mo.

B. Migration barriers

The vast majority of experimental diffusion studies of TMs in silicon has been devoted to the 3d-row elements. Most of these species are believed to migrate through the lattice via a direct interstitial mechanism with reported energy barriers in the 0.4–1.0 eV range [9]. Although several 3d metals are fast diffusers in Si, diffusion data display strong differences in diffusivity across the 3d row with an increase in diffusivity by almost five orders of magnitude from Ti towards the rightmost TMs, Ni, and Cu. Whereas, Cu possesses the largest diffusion

coefficients observed in silicon, Ti and V on the other side are well known slow diffusers and difficult to remove by standard gettering techniques [23,67]. Previous calculations [9,68,69] based on empirical models of interatomic interactions have provided migration energies of the order of 1 eV and less. Nonetheless, the empirical nature of these models means that their predictions should be viewed as qualitative estimates. A comprehensive first-principles study of migration barriers of transition metals in silicon was presented by Kamon *et al.* [20]. These authors determined the migration barriers for interstitial diffusion for all 3d-row metals within DFT in the LDA. They did not consider, however, spin polarization and made use of rather small-size silicon supercells with sixteen atoms. The obtained barriers overestimated the experimentally reported ones by a factor of two. In contrast, the recent DFT calculations of Backlund and Estreicher [23] for Ti made use of considerably larger supercells and provided migration barriers (in both its neutral and positively-charged states) in much better agreement with the experimental data.

In the present study, we report both DFT and DFT+U calculations of the migration barriers for diffusion of the early 3d- and 4d-row TMs in silicon. It is assumed that a direct interstitial diffusion is the dominant mechanism for these TMs. Accordingly, the metal performs consecutive atomic jumps between adjacent tetrahedral interstitial sites (T) through the hexagonal (H) site of the Si lattice, which is assumed to be the saddle-point along the migration configurational space. We checked this assumption by marginally displacing the TM away from the H site and verified that the impurity attained the T site after full relaxation. The magnitude of the migration barrier was then determined as the difference between the total energies of fully relaxed defects at the T and H interstitial sites. In these calculations, we also assumed that the total spin of the TM is conserved during the migration step, remaining equal to its value obtained in the ground state (at or near the tetrahedral site). Two charge states, the neutral and singly positive were considered for each species, a choice which covers a wide range of doping conditions. Within DFT+U, the corresponding on-site Hubbard and Hund parameters were then taken specifically for the charge/spin states considered (see Fig. 2). The only exception was for the positively-charged state of vanadium, V^+, which adopts a HS ($S = 2$) configuration within DFT+U. In this case, the corresponding U and J parameters were again generated for this specific state. The obtained U and J values were equal to 3.7 and 0.9 eV, respectively. These are to be compared to $U = 3.7$ eV and $J = 2.2$ eV obtained for the LS $^1V^+$ state.

The results for all positively-charged and neutral metals are listed in Table III. For some of them (Ti, Cr, and Zr), the magnitude of the barriers exhibits a weak dependence on the charge state. V, Nb, and Mo, on the other hand, show considerable charge-state effects in their migration barriers (V only within DFT+U and Nb within DFT). For Nb and Mo, the DFT barrier for the neutral state exceeds that of the positively charged state by 0.3 eV. This also holds for the DFT+U barriers of V. For Mo, this finding is reversed within DFT+U with the barrier for its positively charged state being larger by about 0.4 eV. Correlation effects are also moderate in most cases. For the metals with the smaller effective interaction, $U - J$, (namely, Cr, Zr, and Nb) the differences among DFT and DFT+U values do not exceed 0.20 eV. For the other metals the differences between DFT and DFT+U barriers are a bit higher than 0.20 eV (Ti and V) and attain their largest magnitude for the case of the neutral state of Mo (about 0.6 eV).

TABLE III. Migration barriers of the early 3d and 4d TMs in silicon obtained by DFT and DFT+U (values in eV). For each TM the corresponding spin values S and charge states q are shown as left and right superscripts on the species symbol. For the positively-charged V, the DFT and DFT+U results correspond to its LS and HS states, respectively. Experimental (Exp.) values are also shown for comparison.

3d row	$^1Ti^0$ / $^{3/2}Ti^+$	$^{1/2}V^0$ / $^SV^+$	$^2Cr^0$ / $^{5/2}Cr^+$
DFT	1.98 / 1.94	1.30 / 1.41 ($S = 1$)	0.77 / 0.74
DFT+U	1.74 / 1.81	1.52 / 1.19 ($S = 2$)	0.72 / 0.72
Exp.	1.79[a]	1.55[b]	1.0[c], 0.85[d]
4d row	$^1Zr^0$ / $^{3/2}Zr^+$	$^{1/2}Nb^0$ / $^1Nb^+$	$^0Mo^0$ / $^{1/2}Mo^+$
DFT	2.29/2.30	2.52/2.23	2.31/2.01
DFT+U	2.48/2.42	2.44/2.42	1.70/2.08
Exp.	–	–	2.2[e]

[a]Reference [70].
[b]Reference [71].
[c]Reference [72].
[d]Reference [73].
[e]Reference [74].

Among the 3d-row TMs it can be seen that Ti possesses the largest migration barriers (by either DFT and DFT+U) something that confirms its observed behavior as a slow diffusing impurity in silicon [8]. The DFT+U values in this case match better the reported experimental barrier [70]. These measurements were carried out at high temperatures (~1000 °C), with the Fermi level being effectively at midgap. Hence they should be compared to the calculated barrier of $^{3/2}Ti^+$. The present DFT results for Ti also agree reasonably well with previous DFT-GGA calculations [23], which reported barriers of 1.75 and 1.66 eV for the neutral and positively charged states of Ti, respectively. The calculated barriers for V are lower from those of Ti but still they are above of 1 eV. The barrier of V^0 exhibits some small dependence on the on-site correlation, with the DFT+U result (1.52 eV) agreeing better to the experimental value [71] (1.55 eV). Regarding V^+, correlation effects are also observed, with the DFT+U barrier of the HS $^2V^+$ state lower by about 0.2 eV with respect to the DFT one. Here, however, it is important to note that the DFT+U result refers to the HS $S = 2$ state, which is the ground state of V^+ within this method (see Sec. III A). The calculated barrier for the LS $^1V^+$ within DFT+U was found equal to 1.24 eV, very close to the magnitude of its HS counterpart. Cr possesses the smallest migration barriers among the metals studied. In an early report, the barrier for Cr diffusion in silicon was measured as 1 eV [72]. However, more recent experiments performed on p-type materials for an extended temperature range (down to room temperature), resulted in a migration barrier of 0.85 eV [73]. This value should represent the migration barrier of Cr^+, and matches well our calculations.

The 4*d*-row TMs also possess high migration barriers, surpassing those of their 3*d*-row counterparts due to their larger size. The calculations suggest that the early 4*d* TMs examined here should also be slow diffusers, something that is known from experimental reports for Mo [55,74]. Furthermore, the migration barrier of 2.2 eV extracted for Mo from depth profiling measurements on Mo-implanted silicon [74], matches well the present results (see Table III).

IV. CONCLUDING REMARKS

We carried out a systematic study of the electrical levels and migration barriers of six early 3*d*-row and 4*d*-row TMs in silicon. By employing both a semilocal DFT functional and a rotationally invariant DFT+U approach, our analysis includes the effects of on-site correlation within the *d*-electron shell of each TM. The on-site Hubbard U and J parameters were determined self-consistently from linear response theory taking full account of the screening of the host and local bonding around the impurity. This procedure avoids ambiguities originating from alternative approaches that employ fitting to experimental data. It also provides a physically intuitive picture of the relative importance of on-site Coulomb and exchange effects. Although the present methodology is shown to work reasonably well for the early TMs in Si, there are still insufficiencies to be addressed. Perhaps the most severe one is the well-known underestimation of the gap inherent to (semi)local DFT functionals; in the present case, the on-site U and J corrections have a local effect on the TM, and not on the host. In this respect, a combination of the present approach with a more accurate hybrid-type functional could be promising [7].

Strong correlation effects were observed for the calculated levels of the 3*d* TMs, mainly Ti and V, which possess the largest U parameters. For V in particular, inclusion of on-site correlation changed the spin ordering for the positively-charged state, leading to a high-spin $^2V^+$ ground state. The single-donor and acceptor levels were far more affected owing to the accumulated correlation which increases with the addition of electrons to the TM *d*-shell. In contrast, for the 4*d* metals, on-site correlation effects were relatively small and scaled with the magnitude of the effective interaction $U - J$, whose range was between 1 eV (for Zr) and 2 eV (for Mo). For all TMs, the agreement to the experiments is deemed satisfactory, confirming the presence of three deep levels in the gap for the metals of the two leftmost columns, Ti/Zr and V/Nb. For Cr, both DFT and DFT+U results reproduce well the experimentally established single-donor level in the upper part of the gap. Furthermore, no stable double-donor level is predicted for Cr by either functional, thus resolving a long-standing controversy in a number of experimental studies. For Mo, the present calculations identify the well-established donorlike level at $E_V + 0.30$ eV as a single-donor type, Mo(0/+), rather than a double-donor one, Mo(+/++). The latter, instead, is found to edge the VB top.

The present study also provides first-principles calculations of migration barriers of the early TMs in silicon. Charge-state effects were found to be rather small with the exception of Nb (only within DFT), V, and Mo. Correlation effects were moderate in most cases, with the larger differences observed for those metals showing larger on-site Coulomb U parameters, namely Ti, V, and Mo. Among the 3*d*-row metals, high barriers were obtained for Ti and V in very good agreement with the experiments. Cr on the other hand was found to possess considerably smaller migration barriers in the 0.72–0.77 eV range (depending on its charge state), also matching quite well the experimentally reported value (0.85 eV). As a matter of fact, considering that (i) the migration barrier of Cr is close to those of other fast-diffusing impurities in silicon (like Fe) and (ii) Cr is predicted to have at least a deep donor level, it is likely that this can be a highly detrimental impurity that solar-Si manufacturers should pay more attention to. Finally, all metals from the 4*d* row, Zr, Nb, and Mo, possess larger migration barriers than their 3*d* counterparts, indicating a higher difficulty in passing through the hexagonal ring of the Si lattice. The existing experimental evidence that Mo is a slow-diffusing species supports these results.

ACKNOWLEDGMENTS

This work was funded by FEDER funds through the COMPETE 2020 Programme and by National Funds through FCT - Portuguese Foundation for Science and Technology under the projects UID/CTM/50025/2013 and PTDC/CTM-ENE/1973/2012.

[1] B. Himmetoglu, A. Floris, S. de Gironcoli, and M. Cococcioni, Int. J. Quantum Chem. **114**, 14 (2014).
[2] J. Heyd, G. E. Scuseria, and M. Ernzerhof, J. Chem. Phys. **118**, 8207 (2003).
[3] J. Heyd and G. E. Scuseria, J. Chem. Phys. **121**, 1187 (2004).
[4] J. Paier, M. Marsman, K. Hummer, G. Kresse, I. C. Gerber, and J. G. Angyan, J. Chem. Phys. **124**, 154709 (2006).
[5] P. B. A. Alkauskas and A. Pasquarello, Phys. Status Solidi B **248**, 775 (2011).
[6] P. Deák, B. Aradi, T. Frauenheim, E. Janzén, and A. Gali, Phys. Rev. B **81**, 153203 (2010).
[7] V. Ivády, I. A. Abrikosov, E. Janzén, and A. Gali, Phys. Rev. B **87**, 205201 (2013).
[8] A. R. Peaker, V. P. Markevich, B. Hamilton, G. Parada, A. Dudas, A. Pap, E. Don, B. Lim, J. Schmidt, L. Yu, Y. Yoon, and G. Rozgonyi, Phys. Status Solidi A **209**, 1884 (2012).
[9] E. R. Weber, Appl. Phys. A **30**, 1 (1983).
[10] H. H. Woodbury and G. W. Ludwig, Phys. Rev. **117**, 102 (1960).
[11] G. W. Ludwig and H. H. Woodbury, *Solid State Physics*, edited by F. Seitz and D. Turnbull, Vol. 13 (Academic Press, New York, 1962).
[12] H. Lemke, Phys. Stat. Sol. (a) **122**, 617 (1990).

[13] M. L. Polignano, D. Codegoni, G. Borionetti, F. Bonoli, J. Brivio, S. Greco, A. Marino, P. Monge, I. Patoprsta, V. Privitera, and C. Riva, ECS Trans. **33**, 133 (2010).

[14] G. G. DeLeo, G. D. Watkins, and W. B. Fowler, Phys. Rev. B **25**, 4972 (1982).

[15] D. E. Woon, D. S. Marynick, and S. K. Estreicher, Phys. Rev. B **45**, 13383 (1992).

[16] H. Katayama-Yoshida and A. Zunger, Phys. Rev. B **31**, 8317 (1985).

[17] F. Beeler, O. K. Andersen, and M. Scheffler, Phys. Rev. Lett. **55**, 1498 (1985).

[18] F. Beeler and M. Scheffler, Mater. Sci. Forum **38-41**, 257 (1989).

[19] F. Beeler, O. K. Andersen, and M. Scheffler, Phys. Rev. B **41**, 1603 (1990).

[20] Y. Kamon, H. Harima, A. Yanase, and H. Katayama-Yoshida, Physica B **308-310**, 391 (2001).

[21] Z. Z. Zhang, B. Partoens, K. Chang, and F. M. Peeters, Phys. Rev. B **77**, 155201 (2008).

[22] K. Sánchez, I. Aguilera, P. Palacios, and P. Wahnón, Phys. Rev. B **79**, 165203 (2009).

[23] D. J. Backlund and S. K. Estreicher, Phys. Rev. B **81**, 235213 (2010).

[24] V. P. Markevich, S. Leonard, A. R. Peaker, B. Hamilton, A. G. Marinopoulos, and J. Coutinho, Appl. Phys. Lett. **104**, 152105 (2014).

[25] S. K. Estreicher, D. J. Backlund, C. Carbogno, and M. Scheffler, Angewandte Chemie International Edition **50**, 10221 (2011).

[26] M. Cococcioni and S. de Gironcoli, Phys. Rev. B **71**, 035105 (2005).

[27] S. Lany and A. Zunger, Phys. Rev. B **80**, 085202 (2009).

[28] V. I. Anisimov, J. Zaanen, and O. K. Andersen, Phys. Rev. B **44**, 943 (1991).

[29] J. Morgan and G. W. Watson, J. Phys. Chem. C **113**, 7322 (2009).

[30] A. I. Liechtenstein, V. I. Anisimov, and J. Zaanen, Phys. Rev. B **52**, R5467 (1995).

[31] S. L. Dudarev, G. A. Botton, S. Y. Savrasov, C. J. Humphreys, and A. P. Sutton, Phys. Rev. B **57**, 1505 (1998).

[32] G. W. Ludwig and H. H. Woodbury, Phys. Rev. Lett. **5**, 98 (1960).

[33] E. Bousquet and N. Spaldin, Phys. Rev. B **82**, 220402(R) (2010).

[34] B. Himmetoglu, R. M. Wentzcovitch, and M. Cococcioni, Phys. Rev. B **84**, 115108 (2011).

[35] M. Wierzbowska and A. Fleszar, Phys. Rev. B **83**, 184418 (2011).

[36] G. Kresse and J. Hafner, Phys. Rev. B **47**, 558 (1993).

[37] G. Kresse and J. Hafner, Phys. Rev. B **49**, 14251 (1994).

[38] G. Kresse and J. Furthmüller, Phys. Rev. B **54**, 11169 (1996).

[39] P. E. Blöchl, Phys. Rev. B **50**, 17953 (1994).

[40] G. Kresse and D. Joubert, Phys. Rev. B **59**, 1758 (1999).

[41] J. P. Perdew, K. Burke, and M. Ernzerhof, Phys. Rev. Lett. **77**, 3865 (1996).

[42] P. Giannozzi, S. Baroni, N. Bonini, M. Calandra, R. Car, C. Cavazzoni, D. Ceresoli, G. L. Chiarotti, M. Cococcioni, I. Dabo *et al.*, J. Phys.: Condens. Matter **21**, 395502 (2009).

[43] D. Vanderbilt, Phys. Rev. B **41**, 7892 (1990).

[44] A. Resende, R. Jones, S. Oberg, and P. R. Briddon, Phys. Rev. Lett. **82**, 2111 (1999).

[45] J. P. Goss, M. J. Shaw, and P. R. Briddon, *Marker-Method Calculations for Electrical Levels Using Gaussian-Orbital Basis Sets* (Springer, Berlin, Heidelberg, 2007), Chap. 3, pp. 69–94.

[46] J.-W. Jeong and A. Oshiyama, Phys. Rev. B **64**, 235204 (2001).

[47] J. Coutinho, V. J. B. Torres, R. Jones, and P. R. Briddon, Phys. Rev. B **67**, 035205 (2003).

[48] J. P. Goss, P. R. Briddon, R. Jones, and S. Sque, Diam. Relat. Mat. **13**, 684 (2004).

[49] J. Coutinho, S. Öberg, V. J. B. Torres, M. Barroso, R. Jones, and P. R. Briddon, Phys. Rev. B **73**, 235213 (2006).

[50] S. K. Estreicher, M. Sanati, and N. Gonzalez Szwacki, Phys. Rev. B **77**, 125214 (2008).

[51] G. Makov and M. C. Payne, Phys. Rev. B **51**, 4014 (1995).

[52] C. Freysoldt, J. Neugebauer, and C. G. Van de Walle, Phys. Rev. Lett. **102**, 016402 (2009).

[53] E. K. U. Gross, E. Runge, and O. Heinonen, *Many-Particle Theory* (Adam Hilger, Bristol, 1991).

[54] D. A. van Wezep and C. A. J. Ammerlaan, J. Electron. Mater. **14A**, 863 (1985).

[55] A. Rohatgi, R. H. Hopkins, J. R. Davis, and R. B. Campbell, Solid State Electron. **23**, 1185 (1980).

[56] T. Hamaguchi and Y. Hayamizu, Jpn. J. Appl. Phys. **30**, L1837 (1991).

[57] B. B. Paudyal, K. R. McIntosh, D. H. Macdonald, and G. Coletti, J. Appl. Phys. **107**, 054511 (2010).

[58] T. Sadoh, H. Nakashima, and T. Tsurushima, J. Appl. Phys. **72**, 520 (1992).

[59] H. Feichtinger and R. Czaputa, Appl. Phys. Lett. **39**, 706 (1981).

[60] H. Conzelmann, K. Graff, and E. R. Weber, Appl. Phys. A **30**, 169 (1983).

[61] A. A. Zolotukhin and L. S. Milevskii, Sov. Phys. Semicond. **10**, 914 (1976).

[62] J. R. Davis, A. Rohatgi, R. H. Hopkins, P. D. Blais, P. R. Choudhury, J. R. McCormick, and H. C. Mollenkopf, IEEE Trans. Electron Devices **27**, 677 (1980).

[63] T. Kunio, T. Yamazaki, E. Ohta, and M. Sakata, Solid State Electron. **26**, 155 (1983).

[64] D. Mathiot and S. Hocine, J. Appl. Phys. Phys. **66**, 5862 (1989).

[65] S. M. Cox, ECS J. Solid State Sci. Technol. **3**, P397 (2014).

[66] H. Pettersson, H. G. Grimmeiss, L. Tilly, K. Schmalz, and H. Kerkow, Semicond. Sci. Technol. **8**, 1247 (1993).

[67] R. Singh, S. J. Fonash, and A. Rohatgi, Appl. Phys. Lett. **49**, 800 (1986).

[68] R. A. Swalin, J. Phys. Chem. Sol. **23**, 154 (1962).

[69] J. Utzig, J. Appl. Phys. **65**, 3868 (1989).

[70] S. Hocine and D. Mathiot, Appl. Phys. Lett. **53**, 1269 (1988).

[71] T. Sadoh and H. Nakashima, Appl. Phys. Lett. **58**, 1653 (1991).

[72] N. T. Bendik, V. S. Garnyk, and L. S. Milevskii, Sov. Phys. Solid State **12**, 150 (1971).

[73] J. Zhu, J. Diz, D. Barbier, and A. Laugier, Materials Sci. and Eng. B **4**, 185 (1989).

[74] J. L. Benton, D. C. Jacobson, B. Jackson, J. A. Johnson, T. Boone, D. J. Eaglesham, F. A. Stevie, and J. Becerro, J. Electrochem. Soc. **146**, 1929 (1999).